ACS NANO
Cite This: ACS Nano 2018, 12, 1146–1155
www.acsnano.org
ARTICLE

Localized DNA Hybridization Chain Reactions on DNA Origami

Hieu Bui,[†,§,∥] Shalin Shah,[‡,∥] Reem Mokhtar,[†] Tianqi Song,[†] Sudhanshu Garg,[†] and John Reif*[,†,‡]

[†]Department of Computer Science, Duke University, Durham, North Carolina 27708, United States
[‡]Department of Electrical and Computer Engineering, Duke University Durham, North Carolina 27708, United States
[§]National Research Council, 500 Fifth Street NW, Keck 576, Washington, DC 20001, United States

Supporting Information

ABSTRACT: **The field of DNA nanoscience has demonstrated many exquisite DNA nanostructures and intricate DNA nanodevices. However, the operation of each step of prior demonstrated DNA nanodevices requires the diffusion of DNA strands, and the speed of these devices is limited by diffusion kinetics. Here we demonstrate chains of localized DNA hybridization reactions on the surface of a self-assembled DNA origami rectangle. The localization design for our DNA nanodevices does not rely on the diffusion of DNA strands for each step, thus providing faster reaction kinetics. The locality also provides considerable increased scalability, since localized components of the devices can be reused in other locations. A variety of techniques, including atomic force microscopy, total internal reflection fluorescence, and ensemble fluorescence spectroscopy, are used to confirm the occurrence of localized DNA hybridization reactions on the surface of DNA origami. There are many potential biological applications for our localized DNA nanodevices, and the localization design is extensible to applications involving DNA nanodevices operating on other molecular surfaces, such as those of the cell.**

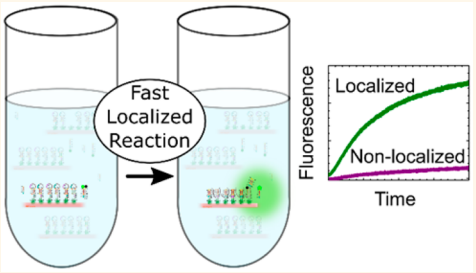

KEYWORDS: *DNA self-assembly, structural DNA nanotechnology, dynamic DNA nanotechnology, DNA nanoscience, DNA hairpins, locality, localized hybridization reactions*

Self-assembly, programmability, and predictability are the most attractive properties of DNA. Since the first demonstration of creating lattices from a finite set of DNA sequences,[1] many exquisite nanoscale structures and intricate devices have been reported.[2−12] There are two major research themes concurrently being explored within the field of DNA nanotechnology. The first can be classified as structural DNA nanotechnology where molecular self-assembly *via* hybridization reactions creates nanoscale molecules that can be expanded to microscale structures.[11] The other is called dynamic DNA nanotechnology where programmable dynamic nanomachines including DNA strand displacement systems are used to produce motion and perform (primitive) computations.[12]

There are multiple exciting potential biological applications[13−15] combining structural and dynamic DNA nanodevices. For instance, the stability of DNA nanostructures in the cellular environment has been explored in multiple studies.[16−18] In addition, DNA nanostructures were designed as intelligent nanomachines to carry RNA,[19] aptamers,[20] vaccines,[21] and drugs[22] to target cellular structures. The ability to perform primitive computation on cellular surfaces may provide the following benefits: (i) the output signals of diffusing systems may interact with other molecules present in solution, whereas the output signals from localized systems are much more likely to be triggered by the adjacent molecules nearby, thereby achieving greater control over directing reaction pathways; (ii) the detection of different extracellular proteins may be enhanced *via* localized DNA circuits due to the flexibility of programming distinct localized DNA gates; and (iii) different pathways of molecules entering or leaving the extracellular and intracellular environments may be investigated with the help of localized DNA circuits. However, DNA hybridization reactions on cellular surfaces have not been extensively investigated.[23]

A feasible approach in this direction is to develop and refine the capability of localized DNA hybridization reactions on self-assembled DNA nanostructures. This would combine the two research themes of structural and dynamic DNA nanostructures to fully exploit the potential of DNA nanotechnology. There have recently been some investigations of localized DNA hybridization reactions on DNA origami nanostructures.[24] Teichmann *et al.* studied the effect of co-localization by immobilizing a two-stage DNA strand displacement reaction onto a DNA origami platform.[25] Kopperger *et al.* studied the diffusive transport of DNA cargo strands bound to a DNA

Received: September 20, 2017
Accepted: January 22, 2018
Published: January 22, 2018

DOI: 10.1021/acsnano.7b06699
ACS Nano 2018, 12, 1146–1155

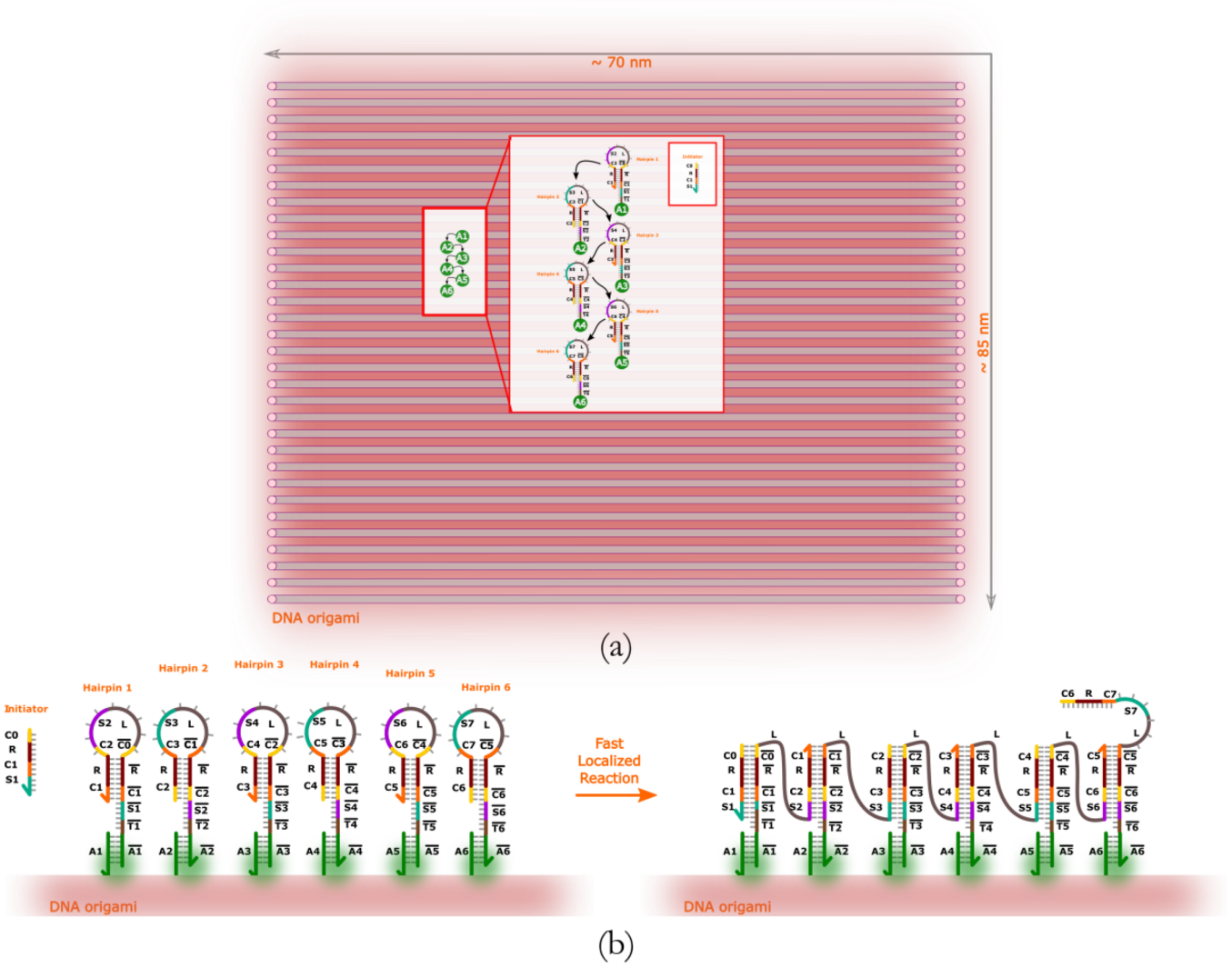

Figure 1. (a) DNA origami rectangle with modified staple strands (green circles). Metastable DNA hairpins tethering to DNA origami rectangle's surface *via* modified staple strands through the anchor domains. (b) Mechanism of DNA hybridization reactions on DNA origami surface.

origami structure.[26] Ruiz *et al.* constructed a simple seesaw DNA amplifier by tethering DNA strands to DNA origamis.[27] Several theoretical works have shown that constraining distances among DNA strands lead to faster reaction rates.[28−30] However, prior works on nondiffusion-based kinetics were either theoretical[27,30] or they required the diffusion of DNA strands in one[26] or more steps of their operation,[25,29,31] and the diffusion kinetics limited the speed of their operation. Furthermore, the global diffusion of DNA strands in each step of their operation also limits the scalability of localized systems. Our earlier work[32] attempted to localize DNA hybridization reactions on a single DNA track, however the ability to incorporate more DNA strands was limited by the finite size of the synthetic single-stranded DNA track.

As mentioned, prior dynamic DNA nanodevices used DNA strands to encode values and DNA hybridization reactions to perform computations, where values were transported during computation using diffusion.[33] During diffusion, DNA molecules randomly collide and interact in a three-dimensional fluidic space. At low concentrations and temperatures, collision frequency can be quite slow and could impede the kinetics of these systems. At higher concentrations and temperature, unintended spurious interactions during diffusion can hinder the computations. Hence, increasing the concentration of DNA strands to speedup DNA hybridization reactions has the unfortunate side effect of increasing leaks, which are undesired hybridization reactions in the absence of input strands. Also, diffusion-based systems possess global states encoded *via* concentrations of various species and hence exhibit only limited ability for parallelization.

Here we present a system to investigate DNA hybridization reactions on the surface of a DNA origami rectangle as a potential route toward performing computation on cellular and other biological surfaces. The proposed system attempts to achieve faster reaction kinetics than in regular DNA hybridization systems. This system combines the large surface area of the DNA origami nanostructure and linearly cascaded DNA hybridization reactions to deliberately achieve localized signal propagation responses. Unlike prior works[25−27] on localized DNA hybridization reactions, the proposed system utilizes the unique properties inherent in DNA hairpins instead of typical gate and signal strands for constructing the linear cascade reaction. DNA hairpins can be programmed to undergo conformational changes while also exhibiting the same desirable

DOI: 10.1021/acsnano.7b06699
ACS Nano 2018, 12, 1146−1155

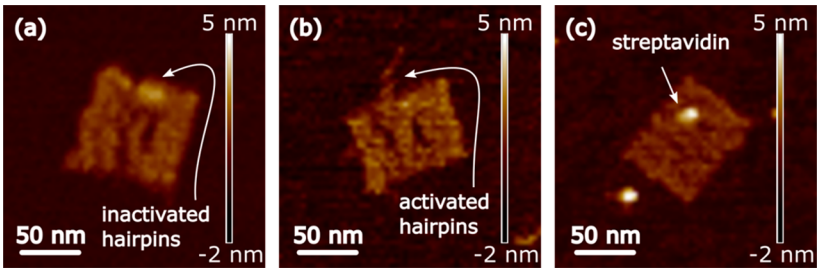

Figure 2. Dry AFM images of DNA origami rectangle labeled with DNA hairpins at thermal equilibrium. Six metastable DNA hairpins self-assembled on DNA origami rectangle (a), after adding the initiator (b), and after adding the biotin-labeled output to detect the reaction completion *via* binding to the streptavidin molecule (c). Refer to SI Figure S2 for additional AFM data.

properties as nonhairpin DNA strands such as responsiveness to external stimuli, that is, DNA strand displacement, as well as mitigating the loss of active components during a reaction.

The DNA origami rectangle design from Rothemund[24] is an ideal candidate for studying the proposed localized DNA hybridization reaction, as shown in Figure 1. The design consists of 224 short staple strands and a long scaffold M13mp18 (refer to SI Figure S1 for details). A subset of staple strands was modified with 24-nt length sticky ends (green circles in Figure 1) to attach DNA metastable hairpins *via* anchor domains (A_i). To study the localized DNA hybridization reaction, a set of distinct metastable DNA hairpins was designed to (i) precisely bind to the surface of the DNA origami rectangle and (ii) be triggered[34] and undergo a cascade DNA hybridization chain reaction in the presence of an external stimulus. Each metastable DNA hairpin consists of a stem, a loop, and a sticky end. The sticky end consists of a spacer domain (T_i), an anchor domain (A_i), and an external domain (S_i). The sticky end serves multiple purposes: (i) to anchor the hairpin to the DNA origami surface *via* the A_i domain and (ii) to encode an external toehold (S_i) for the localized DNA hybridization reaction. The stem consists of two domains (C_i and R) to form a stable duplex with 14 base pairs. The purpose of the stem is to sequester active domains (S_{i+1}) within the loop prior to triggered self-assembly. The loop consists of two clamp domains (C_{i-1} and C_{i+1}), a linker domain (L), and a sequestered domain (S_{i+1}). The two clamp domains were used to prevent a hairpin from reclosing *via* a localized blunt-end displacement once it has been opened near both ends of the hairpin's stem.[35,36] The purposes of the loop are (i) to encode the sequestered domain for the cascade reaction and (ii) to fasten the cargo (S_{i+1}) from floating away to solution. Each hairpin has two toehold domains (S_i and S_{i+1}): S_i is an external toehold domain and readily available for hybridization and S_{i+1} is an internal toehold domain and unavailable for hybridization. It is worth noting that the hairpins were designed to assemble in a zigzag, instead of a linear arrangement, in order to satisfy antiparallel strand directionality within the given design. In particular, odd-numbered hairpins have the same directionality (5′ to 3′) and even-numbered hairpins have the opposite directionality from the odd ones. A linear arrangement with all hairpins having the same 5′ to 3′ directionality can possibly be explored (though it would require changing the set of DNA sequences). Prior studies[25−27] often arranged DNA strands in a linear fashion to enforce the same directionality among DNA strands. Prior studies[26] suggest that changing the position of DNA sequences on DNA origami affects the localized reaction. However, the system reported here does not take into account the effect of changing the position of hairpins instead of focusing on the extensive list of sequence designs to elucidate the benefit of localized cascade reaction.

The mechanism of the localized DNA hybridization reaction is shown in Figure 1b. Initially, all DNA hairpins are bound to the anchor domains on the DNA origami rectangle. Upon adding the initiator, the localized DNA hybridization reaction is initiated. In particular, the initiator hybridizes to the first hairpin H1 *via* domain S_i and displaces H1's stem domain, thus activating its sequestered domain S_{i+1} within its loop. The sequestered domain can now hybridize to the adjacent hairpin H2, resulting in a similar effect. The process continues until the last hairpin H6 is fully opened. The linker domain ensures the two adjacent hairpins interact properly. In particular, the hairpins are far enough that the two domains (S_i of the first hairpin loop and the corresponding S_i* of the second hairpin stem) cannot reach each other until the first hairpin is opened and the linker allows S_i to extend. Without localization to the DNA origami rectangle surface, the hairpins would be expected to complete the cascade reaction slower due to diffusion. In addition, since the proposed system can be operated at low concentration, the leaks—undesired reactions in the absence of input sequences and between two different origami—are expected to be lower than at high concentration.[31,37]

RESULTS AND DISCUSSION

To visualize the self-assembly of DNA hairpins on the surface of a DNA origami rectangle, a solution of DNA origami rectangles mixed with DNA hairpins was imaged using atomic force microscopy (AFM) in dry mode, as shown in Figure 2a. DNA origami rectangles were clearly formed, and six hairpins formed a height feature complex similar to the designated location as illustrated in Figure 1. The initiator was then added to the sample to initiate the localized DNA hybridization reaction. After thermal equilibrium was reached, samples prepared for dry-mode imaging of the solution were then imaged, as shown in Figure 2b. The resulting assembly of six hairpins was expected to form a DNA duplex. Since it is a challenge to observe a DNA duplex *via* AFM, a biotin-labeled output strand was designed to only bind to the last hairpin and was used to detect the completion of the localized DNA hybridization reaction *via* biotin-streptavidin chemistry. Figure 2c shows the result of binding the biotin-labeled output strand to the last hairpin after completion. The biotin-streptavidin complex is present near the location of six hairpins, indicating that (i) the hairpins were successfully self-assembled to the surface of DNA origami rectangle and (ii) the hairpins underwent localized DNA hybridization reactions after initiation. A key control experiment was performed similar to the system in Figure 2c with the exception that the initiator was

DOI: 10.1021/acsnano.7b06699
ACS Nano 2018, 12, 1146−1155

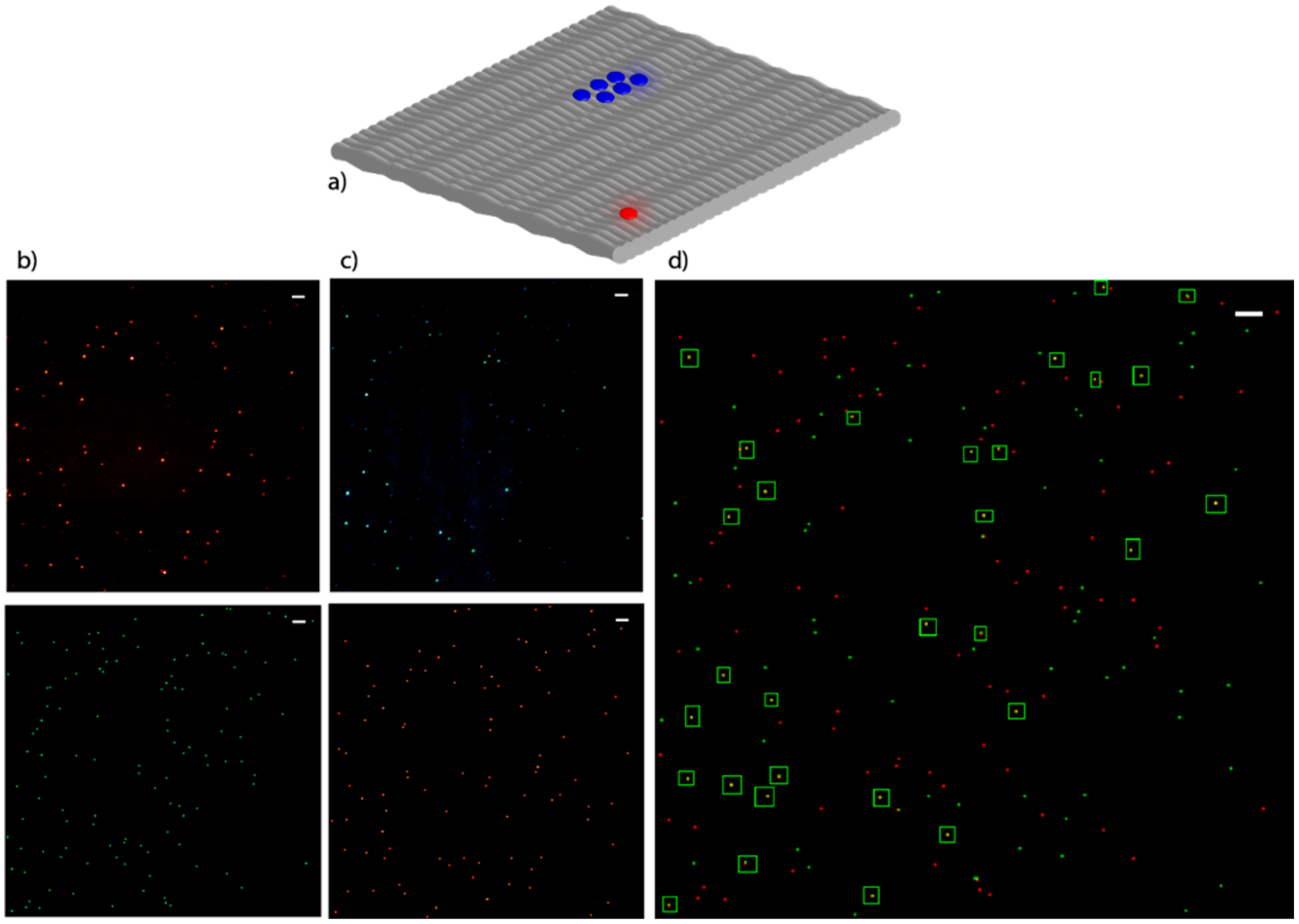

Figure 3. (a) Illustration of DNA origami used single-molecule TIRF experiment. Blue tokens indicate hairpins while red token indicates marker strand. (b, c) TIRF images for DNA origami labeled with ATTO 647N marker and TAMRA initiator. The green channel is for 561 nm laser line (TAMRA label). Similarly, the red channel is for 635 nm laser line (ATTO 647N label). The approximate Gaussian localized images for both the channels. These images are analyzed for co-localization independent of the dynamic range values and noise. (d) Co-localized image where yellow spots (highlighted in green boxes) representing DNA origami with hairpins. Scale bars are 5 μm.

not included. The result of the biotin-labeled output strand binding to the last hairpin after completion did not occur because the localized DNA hybridization reaction was not activated in the absence of the initiator. Without the initiator, the estimated yield of the biotin-streptavidin complex near where the six hairpins could be is 34% less than that with the initiator, as shown in Figure S3. It is worth noting that the high feature complex does not capture or indicate if there is a missing hairpin or multiple missing hairpins on DNA origami rectangles. Based on the scale bar, the length of these activation hairpins should not be so long (Figure 2b), however, the filament-like structure was observed consistently as illustrated in Figure S2b. This behavior results from simply adding the initiator. AFM images were intended to provide a visual inspection of the structures, and it is not a precise representation of the dimension for the reported nanostructures. The yield of all six hairpins assembled on DNA origami is difficult to determine. However, if we assumed the high feature complex on every DNA origami rectangle correlated to the incorporation of hairpins, then the yield of target origami structures was 46% (Figure S3a). The yield of activated hairpins was 40% *via* determining the number of streptavidin-biotin complexes on every DNA origami after adding the initiator (Figure S3c). One caveat of this method is that it does not account for nonspecific binding between the last hairpin and the streptavidin-biotin complex.

To observe equilibrium dynamics of the localized cascade DNA hybridization chain reaction, the solution was characterized using an inverted fluorescence microscope in total internal reflection fluorescence (TIRF) mode (refer to TIRF section in SI for more details). Since the nanostructures of interest are observed below the diffraction limit of light, it is extremely difficult to resolve DNA origami. Therefore, DNA origami with spectrally distinct fluorophores were employed. In particular, ATTO647N fluorophore (excitation and emission peaks at 649 and 662 nm, respectively) was designed to attach to an extended staple strand on DNA origami and was used as a marker for locating DNA origami on the glass surface during TIRF experiments. TAMRA fluorophore (excitation and emission peaks at 559 and 583 nm, respectively) was designed to attach to the first hairpin and used as an initiator to trigger the localized cascade DNA hybridization reaction. To ensure the correct behavior of fluorophore-labeled DNA sequences, a dye-labeled marker strand and a dye-labeled initiator strand were incubated with DNA origami rectangles mixed with DNA hairpins. After filtering excess labeled strands, TIRF images were collected in both channels corresponding to each dye emission fluorescence. To eliminate noise and dependence on

DOI: 10.1021/acsnano.7b06699
ACS Nano 2018, 12, 1146−1155

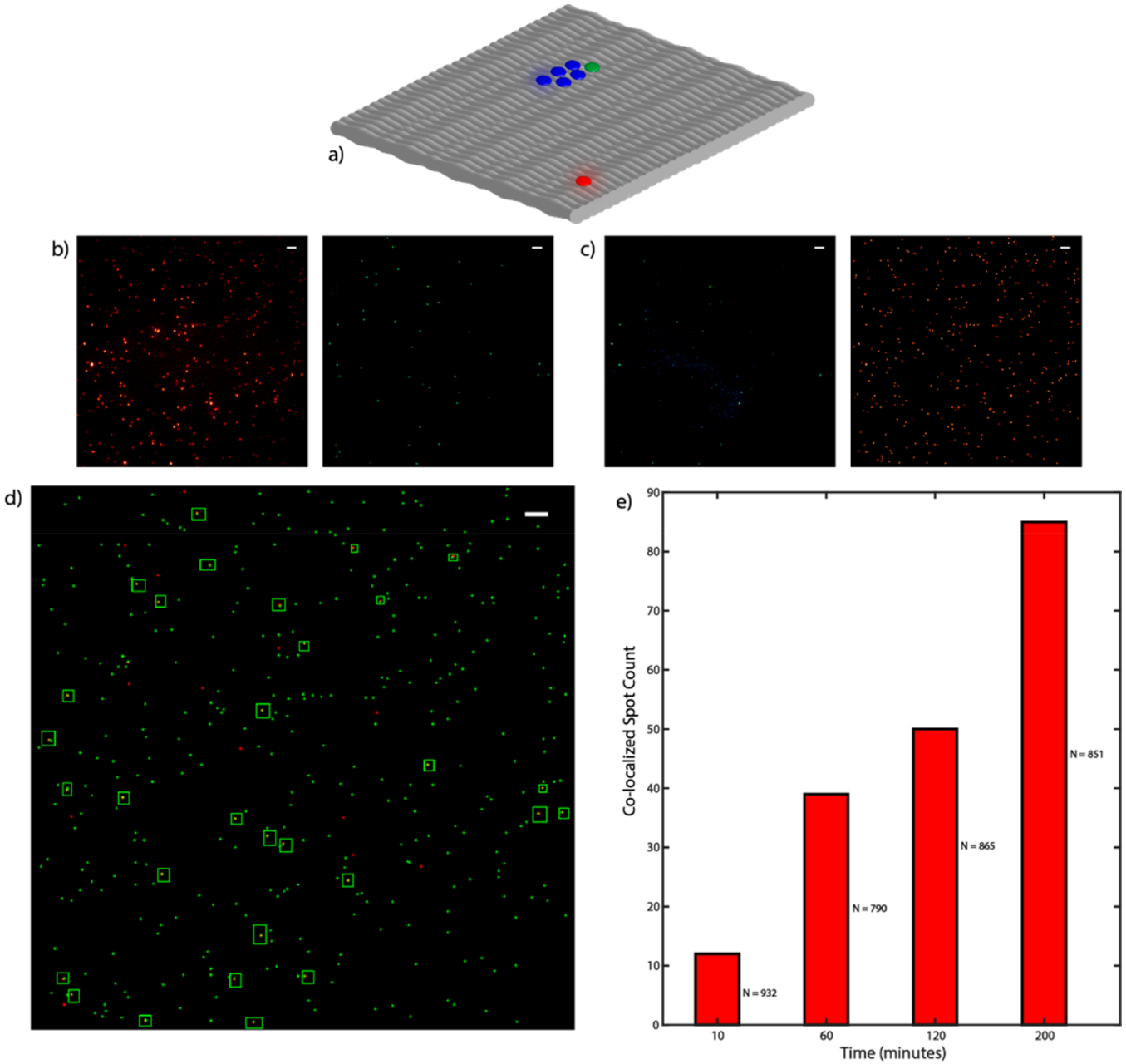

Figure 4. (a) Illustration of DNA origami used single-molecule TIRF experiment. Blue tokens indicate hairpins while red token indicates marker strand. (b, c) TIRF images for DNA origami labeled with ATTO 647N marker dye and ATTO 488 output. The blue channel is for 488 nm laser line (ATTO 488 label). Similarly, the red channel is for 635 nm laser line (ATTO 647N label). The approximate Gaussian localized images for both the channels. (d) Co-localized image where yellow spots (highlighted in green boxes) indicates DNA origami with reaction completion. (e) Co-localization analysis for different reaction incubation times to observe kinetics. Scale bars are 5 μm.

dynamic value range, we performed threshold-based filtering and 2D Gaussian localization for each spot that qualified, as shown in Figure 3b (refer to the single-molecule localization section in SI). These TIRF images were co-localized to detect well-formed DNA origami structures with both marker and initiator attached, as shown in Figure 3c. The co-localized spots, yellow in color, indicate a successful identification of multi-labeled DNA origami with hairpins immobilized on the glass surface with biotin-streptavidin chemistry. For improved visibility, co-localized spots are highlighted with green boxes (refer SI for high-resolution images). The co-localized image shown in Figure 3c suggests that ~15% (approximately 32 out of 213 total localizations; 130 in the red channel and 115 in blue channel) of the DNA origami structures have both the marker and initiator attached.

Since the AFM and TIRF data support the successful formation of DNA origami with labeled hairpins, an output strand was designed to be complementary to the terminal hairpin after the completion of the localized cascade DNA hybridization chain reaction and was labeled with ATTO 488 fluorophore (excitation and emission peaks at 495 and 520 nm, respectively) in order to detect the completion process. Therefore, a solution of DNA origami with hairpins was incubated with 10× unlabeled initiator strand, ATTO 488 labeled output strand, and ATTO 647N labeled marker strand. To observe the dynamic behaviors at different time points, the

DOI: 10.1021/acsnano.7b06699
ACS Nano 2018, 12, 1146−1155

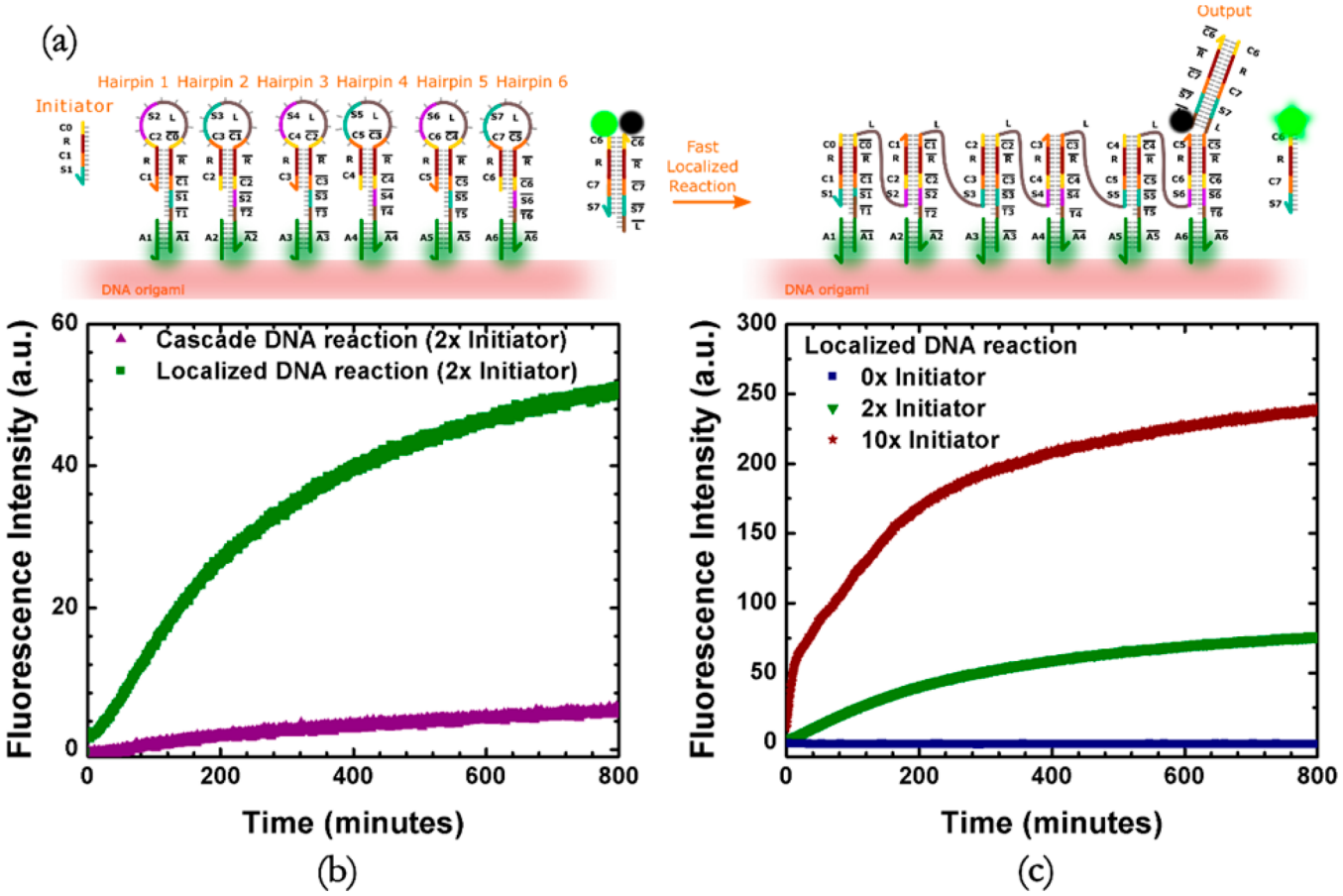

Figure 5. (a) Schematic of localized cascade DNA hybridization chain reaction on the surface of DNA origami rectangle before and after the completion. (b) Kinetic characterization of localized cascade DNA hybridization chain reaction on DNA origami rectangle (green curve). Kinetic characterization of cascade DNA hybridization chain reaction without DNA origami rectangle (purple curve). Each solution was kept at 5 nM concentration and the initiator was added in 2× excess. (b) Effect of localized cascade DNA hybridization chain reaction rate as a function of initiator concentration.

strands were incubated at different time intervals, and the excess strands were filtered using centrifugation method. Figure 4a,b shows co-localization of blue and red channels after 120 min of incubation, indicating that the localized cascade DNA hybridization reaction has reached completion *via* the co-localization spots. The plot for co-localized spots count percentage of total population at 10, 60, and 120 min shows an expected increasing trend, as illustrated in Figure S7. Without removing excess dye-labeled strands in a solution consisting of DNA origami with hairpins, a similar experiment was performed. Similar postprocessing and co-localization analysis demonstrate an increase in the number of spots over time, as shown in Figure 4d. A control experiment for the system in Figure 4d was performed in the absence of the initiator after 200 min of incubation time. As shown in Figure S8, the detected co-localization was significantly less without the initiator (0.4%) as compared to the presence of an initiator (4.5%), indicating that the hairpins reacted considerably less in the absence of the initiator.

Each fluorescence molecule was excited with its corresponding excitation wavelength. The emission from each dye confirms that the dyes were incorporated on the surface of DNA origami, indicating that (i) the emission from the marker dye confirms the observed DNA nanostructures adhered to the glass surface and within the laser evanescent field, otherwise the TIRF effect would result in no emission, (ii) the emission from the initiator dye confirms the initiation of the localized DNA hybridization reaction, and (iii) the emission from the output dye confirms the localized DNA hybridization reaction reached completion. Due to the fast localized nature of the reaction, the TIRFM was not able to capture the reaction rate. However, it should be noted that the ability to detect single-molecule outputs after approximately 10 min is an indication that the actual reaction happens much faster. The increase in spots over time is an indication that the diffusion rate of the initiator and reporter are the likely bottle-necks for reaction observation. Perhaps a special laser setup and a different design with a photoresponsive molecule such as azobenzene[38] to open first hairpin and initiate reaction can be used to achieve more accurate kinetics since there will be no diffusion of initiator involved. One can also use super-resolution techniques such as DNA-PAINT[39] to pattern DNA origami and detect it instead of using multiple dyes and their co-localization. Finally, a recent single-molecule technique with enhanced plasmonic fluorescence[40] can also be used to monitor single molecule reactions with high accuracy. However, it will be challenging to observe reaction progression over time if photobleaching is permitted.

Ensemble fluorescence spectroscopy was also performed to observe the kinetics of the localized DNA hybridization reaction. A fluorescence reporter complex pair was utilized to observe changes in the kinetics of a localized cascade DNA hybridization chain reaction. In particular, the reporter complex

DOI: 10.1021/acsnano.7b06699
ACS Nano 2018, 12, 1146−1155

binds to the last hairpin when it is opened, signifying the chain reaction was completed (illustrated in Figure 5a). Upon adding the initiator to the solution, the fluorescence emission rapidly increased and saturated after 200 min, as shown in Figure 5b (green curve). A control experiment was performed in the absence of the origami rectangle. Upon adding the initiator to the solution, the fluorescence emission was increased slowly, as shown in Figure 5b (purple curve). The ensemble fluorescence response was significantly stronger for the cascade reaction in the presence of the origami rectangle than in the absence of the origami rectangle. This indicates that constraining DNA hairpins onto DNA origami rectangles of the same cascade reaction enhanced the reaction rate. The localized cascade reaction reached 50% completion within 200 min, whereas the cascade reaction in the absence of DNA origami rectangle was slowly increased even after 800 min. The localized DNA reaction is faster than the normal cascade reaction, however, it is a challenge to estimate the effective local concentration on the origami since the signal from the normal cascade reaction does not reach equilibrium within the same timescale. This paper does not attempt to calculate exact kinetic rates or the precise rate increase obtained from localization. Instead, it attempts to show that there is indeed an increase in rates as a result of localization. From our prior studies,[32] it was estimated that the concentration of free DNA solution needs to be increased by a factor of 6 to reach the same effective level of designed localized concentration. In addition, the reaction time for cascade DNA reaction in buffer was faster in the absence of the anchor domains, as reported in the prior studies.[32] In the presence of the anchor domains, however, the reaction time is too long to reach equilibrium for cascade DNA reaction in the buffer, as illustrated in Figure 5b as well as in the prior studies.

Since the initiator was not tethered onto DNA origami, displacing the first hairpin could be the rate-limiting process. To observe the effect of localized cascade DNA hybridization reaction rate as a function of initiator concentration, various concentrations of the initiator were tested, as shown in Figure 5c. At 0× initiator, the fluorescence emission was minimal, indicating that the localized cascade DNA hybridization chain reaction was not significant (blue curve). At 10× (50 nM) initiator, the fluorescence emission was rapidly increased compared to 2× (10 nM) initiator, indicating that the rate-limiting step may be responsible for slowing down the speed of the localized reaction. To overcome the rate-limiting process of initiating the localized cascade DNA hybridization chain reaction, photoactivation mechanisms such as photocleavable molecules could be explored as a replacement method. This result also indicates that displacing the reporter complex by the last hairpin could also be limited by the rate-limiting process. The reporter complex could be tethered to a DNA origami platform to minimize the rate-limiting process. In fact, a fluorescent base (2-aminopurine) was modified to the last hairpin as an alternative approach to overcome the rate-limiting step; however, the fluorescence emission was significantly minuscule for concentration <1 μM (data not shown). In addition, the fluorescence level at 800 min with 2× initiator is much lower than that with 10× initiator. It is worth to note that both 2× and 10× initiator should trigger the reaction cascade to the same completion level. At the end of each experiment, an addition of 10× I6 strand (with domains S6 C6 R C5) was added to directly bind to the last hairpin H6, as shown in Figure S10. These results indicate that the reaction with 2× initiator was much slower than expected. This could be due to an imperfect incorporation of hairpins into the origami even with the same structure. Recently, Chatterjee *et al.* reported a strategy that uses a spatial organization with DNA hairpins laid out on a DNA scaffold.[31] Although the signal propagation was a partially localized architecture, the speed of the circuits is actually much faster than that shown in Figure 5. This could be due to the differences in design strategies: (i) directly attaching hairpins to DNA origami, (ii) utilizing the same intermediate hairpin, and (iii) multiple rounds of purification. These strategies may remove the defects and enhance the yield of functional structures. In addition, the nonlocalized components were added in excess. This effectively drives the reaction similar to a fully localized architecture.

CONCLUSION

This paper presented a potential framework for DNA computation called a localized hybridization network, where diffusion of DNA strands does not occur. (In contrast, all prior attempts to do localized DNA computation have required some diffusion of DNA strands during intermediate stages of the computations.) Instead, all the DNA strands are localized by attaching them to DNA origami which provided an addressable substrate for the strands.

The experiments demonstrated that DNA hairpins were successfully self-assembled to the surface of a DNA origami rectangle. In addition, the hairpins were successfully programmed to undergo cascade DNA hybridization chain reaction on the surface of DNA origami rectangle *via* AFM, TIRF, and ensemble fluorescence spectroscopy.

It is also shown that the speed of DNA hybridization reactions by tethering DNA hairpin sequences to the surface of a DNA origami rectangle has a significant speedup compared to DNA hybridization reactions in the absence of any DNA origami surface. This indicates that localization increases the relative concentration of the reacting DNA strands thereby speeding up the kinetics. This paper demonstrated a localized hybridization network that executed a chain reaction of six DNA hybridizations which executes faster than nonlocalized DNA reactions.

With the advantage of controlling the reaction rate on the surface, the proposed system may be used in the future to target surface-bound proteins and perform computation on cellular membranes. The potential of DNA nanotechnology toward biological applications may be soon realized in disease detection and prevention, whereas DNA logic circuits can be attached to the cell surfaces to communicate changes in extracellular and intracellular activities. For example, detection of proteins will rely on DNA sequences that trigger a localized computation, and the output of this computation will be a fluorescence emission or colorimetric change.

METHODS

Assembly of DNA Origami Rectangle. DNA origami rectangle was designed using caDNAno. A 7249 nt long DNA sequence was derived from the genome of the bacteriophage Mp13mp18 and was used as a scaffold. Staple strands, extended staple strands, and dye-labeled oligonucleotides were purchased from Integrated DNA Technologies, USA. The scaffold M13mp18 was purchased from Guild BioSciences. All sequences and modifications are listed in the SI. DNA hairpins were purified using 10% denaturing polyacrylamide gel electrophoresis (PAGE) prior to self-assembly to DNA origami rectangles. DNA origami structures were folded in a one-pot thermal annealing reaction (from 90 to 22 °C within 90 min) at 100 nM scaffold concentration and 1000 nM (10× molar excess over the

DOI: 10.1021/acsnano.7b06699
ACS Nano 2018, 12, 1146−1155

scaffold) for each structural staple and 5000 nM (20× molar excess) for modified staple strands, which were used for the attachment of the localized DNA hybridization chain reactions. Staples at both ends of the origami structure were left out to prevent blunt-end stacking. The folding buffer contained 12.5 mM magnesium acetate and 1× TAE (40 mM Tris, 20 mM acetic acid, 1 mM EDTA, pH 8.0) and was also used for further sample preparation. For purification of the folded origami structures (removing excess DNA staple strands), 40 μL of DNA origami rectangle mixture at 12.5 mM TAE Mg^{2+} was mixed with 40 μL of 15% PEG 8000 (w/v) at 12.5 mM TAE Mg^{2+}. The sample was mixed by tube inversion without generating air bubbles and spun at 13,000*g* for 25 min. The supernatant was pipetted and discarded. The remaining pellet was dissolved in 12.5 mM TAE Mg^{2+} for 8 h. After removing excess staple and modified staple strands, a mixture of DNA hairpins was added to DNA origami rectangles with extended staple strands in 4× excess. The solution was left overnight, and 15% PEG 8000 (w/v) was performed to remove excess hairpin strands. The PEG purification procedure was done similarly to the step mentioned above. Finally, this PEG purification process was repeated for ATTO 647N labeled marker strand.

The samples for Figures 3, 4, and S8 were further incubated with excess labeled strands at 37 °C for the given time, and excess labeled strands were removed, thrice, using Amicon Ultra centrifugal devices (100,000 MWCO, 13,000*g* speed, 10 min, 4 °C). For all other TIRF samples, incubation was performed at room temperature, and no filtration was performed to remove excess labeled strands.

Atomic Force Microscopy (AFM). Imaging of individual origami DNA nanostructures using AFM was carried out with a Bruker Multimode VIII scanning probe microscope. Five μL of nanostructure solution at 5−10 nM was deposited to a freshly cleaved mica surface. After an addition of 20 μL of 1× TAE Mg^{2+} buffer, the solution was incubated for 5 min at room temperature, then rinsed with 100 μL DI water thrice, and dried with nitrogen gas. ScanAsyst mode was used to image DNA nanostructures in the dry mode using Bruker microcantilever DNP-10C probes.

Total Internal Reflection Fluorescence Microscopy (TIRFM). For specific binding of DNA origami rectangles to the glass surface, biotin/streptavidin chemistry was used. In particular, three staple strands were extended at the 5′ end with biotin modification (see Table S1 and Figures S1 and S5). A 35 mm covered glass slide (MatTek Corporation, USA), with 7 mm well diameter and #1.5 coverslip was used. The Petri dish was rinsed with 500 μL of buffer A (10 mM Tris-HCL, 100 mM NaCl, 0.1% (v/v) Tween 20, pH 8.0) thrice. After a final rinse, 100 μL of 1.0 mg/mL biotin-labeled bovine serum albumin (BSA) was incubated on the glass slide for 5 min. After washing the glass slide, again, with 500 μL of buffer A, 50 μL of 0.5 mg/mL streptavidin was incubated on the glass slide for 5 min. Excess streptavidin was removed by washing once with 500 μL of buffer A and once with 500 μL of buffer B (10 mM Tris-HCL, 10 mM $MgCl_2$, 1 mM EDTA, 0.1% (v/v) Tween 20, pH 8.0). On this passivated glass slide, 50 μL of DNA origami solution (approximately 100 pM in concentration) in 1× TAE Mg^{2+} buffer was incubated for 5 min and washed with buffer B twice to remove excess. Buffer B was used as imaging buffer.

For TIRF samples without centrifugal filtration, we performed imaging using custom-built flow chamber as suggested in prior work.[39,41] A double-sided tape spaced ∼1 mm was attached to a glass slide to attach the coverslip. After removing the excess tape, we used flow-chamber with ∼20 μL volume. Since a flow-chamber can likely remove all the unlabeled strands through washing steps, this is a preferred method when excess labeled ssDNA are not filtered prior to sample preparation for TIRF imaging.

To perform far-field microscopy, Leica DMI 6000B motorized inverted fluorescence microscopy was used in total internal reflection mode with an objective lens (100×, NA = 1.46) in immersion oil. To collect fluorescence from the sample, Hamamatsu (C9100-13) Electron Multiplying Charge Coupled Device (EM-CCD) was used because of its single photon collection capabilities. By using a 100× objective, a pixel size of approximately 228 nm was achieved. To excite fluorescent dyes, laser diodes with 488 nm (10 mW), 561 nm (20 mW), and 635 nm (18 mW) wavelength were used. Fluorescence emissions from fluorescent dyes were filtered through the VBG triple filter (Volume Bragg Gratings - x490/20 d435 m465/45 | x422/44 d505 m545/55 | x552/24 d550 m610/65) and Cy5 filter (x 620/60 d660 m700/75). Each image was collected at 7−9 mW laser power, relatively long exposure time of 1−2 s, and 300 EM gain. Several penetration depths and TIRF angles were tried to achieve best contrast and maximum illumination.

In Figure S6a, the top image represents sample containing 1× PBS as imaging and washing buffer, while the bottom image demonstrates enhanced surface passivation by using buffer A/B for washing and imaging.

Simulations. To predict the behavior of our system, we used the beta version of Microsoft's Visual DSD tool[30] with its added support for simulating tethered DNA circuits. We assumed 5 nM DNA origami concentration, where each origami contains one unit of the localized circuit. In order to achieve better approximation, the rate constants for DNA hybridization and strand displacements were adopted from prior works.[37,42] We simulated our system for 800 min and collected 1000 sample at several initiator concentrations (refer to Figure S9).

Ensemble Fluorescence Spectroscopy. Ensemble fluorescence spectroscopy was used to monitor the kinetics of DNA hybridization reaction in solution and on the surface of the DNA origami. A reporter complex consisting of a fluorophore (TET) and a quencher molecule (FQ) was used to monitor the reaction completion (they were ordered from IDTDNA with HPLC purification and no further purification was done). Only the last hairpin when activated binds to the reporter complex to trigger the fluorescence emission. An equimolar solution of hairpins was mixed together. The fluorophore was excited at 524 nm and emission measured at 541 nm. The excitation and emission slits were set at 10 and 5 nm, respectively. For each experiment, 80 μL of sample (5 nM of DNA hairpins, 6.5 nM of reporter complex) was filled into a clean fluorescence cuvette. All measurements were performed at 20 °C. For kinetic measurements, 1−10 μL of initiator strand was added to an 80 μL sample. Rapid mixing was achieved by carefully but quickly pipetting the whole volume for a minute without generation of air bubbles or loss of material. All experiments were performed in 1× TAE Mg^{2+} buffer solution.

Background Fluorescence for Single-Molecule Imaging. To achieve a good signal-to-noise ratio (SNR), we used a fluorescence microscope in TIRF mode. As shown in Figure S4, these systems have an exponentially decaying evanescent excitation wavefront that ensures selective excitation of molecules extremely close to the surface. This is shown in Figure S4 by decrease in intensity of red spots. In addition, sufficient GC content in our strands ensures fluorescence quenching of free-floating labeled strands. This behavior is demonstrated using ensemble fluorescence graph for ATTO 647N labeled marker strand, in Figure S5. Similar effects have been observed in some prior works.[39,41] The blue curve indicates 100 nM solution of labeled ssDNA, while the orange curve indicates solution containing 100 nM labeled ssDNA and its complementary strand.

Nonspecific Binding. To mitigate the effects of nonspecific binding, we used a two-way blocking mechanism since it has been reported,[43,44] earlier, to reduce the amount of unwanted sticking to the surface. The first component is BSA which is added in the form of biotin-labeled BSA (1 mg/mL), and the second component is Tween 20 which is dissolved in our washing and imaging buffers at 0.1% (v/v). Figure S6 demonstrates the blocking effect of this buffer system for 1 nM marker strand labeled with ATTO 647N, added to the glass surface, without adding any DNA origami. The image on the left has 1× PBS buffer (302 spots), while the one on right containing BSA and Tween 20 (96 spots).

In addition to changing buffer, we performed ultracentrifuge filtration, thrice, prior to adding DNA origami on the glass surface to remove excess labeled ssDNA. There is a clear difference in the blink pattern (refer to supplementary videos).

Single Molecule Localization. Raw images from TIRF machine contain noise and are highly dependent on the dynamic range values, which make them unqualified for any further analysis. Therefore, we used a wavelet filter along with intensity-based thresholding to isolate

DOI: 10.1021/acsnano.7b06699
ACS Nano 2018, 12, 1146−1155

the spots. Each qualified spot was approximated with 2D Gaussian localization since they are a good approximation of Airy disks. This localized image is visualized using average shifted histograms without any pixel magnification to achieve low uncertainty (<5 nm). This final image generated was used for co-localization analysis. All the operations were performed using ThuderSTORM plugin for ImageJ.[45]

ASSOCIATED CONTENT

Supporting Information

The Supporting Information is available free of charge on the ACS Publications website at DOI: 10.1021/acsnano.7b06699.

Details of DNA sequences, additional TIRF data, additional AFM data, additional ensemble fluorescence data, and simulation codes (PDF)

Supplementary TIRF videos and caDNAno design files (ZIP)

AUTHOR INFORMATION

Corresponding Author

* E-mail: reif@cs.duke.edu.

ORCID

Hieu Bui: 0000-0002-1018-761X

Tianqi Song: 0000-0002-0458-3747

Author Contributions

‖These authors contributed equally.

Funding

CCF-1217457, CCF-1141847, CCF-1617791, and CCF-1320360.

Notes

The authors declare no competing financial interest.

ACKNOWLEDGMENTS

The authors thank Zauscher's laboratory for using AFM microscope and Y. Gao of Duke LMCF for imaging advice. The authors wish to thank B. Petkov and D. Fu who assisted in the proof-reading of the manuscript. The authors thank the support from NSF CCF-1617791 and NSF CCF-1320360.

REFERENCES

(1) Seeman, N. C. Nucleic Acid Junctions and Lattices. *J. Theor. Biol.* **1982**, *99*, 237−47.

(2) Bath, J.; Turberfield, A. J. DNA Nanomachines. *Nat. Nanotechnol.* **2007**, *2*, 275−284.

(3) Liedl, T.; Sobey, T. L.; Simmel, F. C. DNA-based Nanodevices. *Nano Today* **2007**, *2*, 36−41.

(4) Modi, S.; Bhatia, D.; Simmel, F. C.; Krishnan, Y. Structural DNA Nanotechnology: From Bases to Bricks, From Structure to Function. *J. Phys. Chem. Lett.* **2010**, *1*, 1994−2005.

(5) Nangreave, J.; Han, D. R.; Liu, Y.; Yan, H. DNA Origami: A History and Current Perspective. *Curr. Opin. Chem. Biol.* **2010**, *14*, 608−615.

(6) Shih, W. M.; Lin, C. X. Knitting Complex Weaves With DNA Origami. *Curr. Opin. Struct. Biol.* **2010**, *20*, 276−282.

(7) Pinheiro, A. V.; Han, D. R.; Shih, W. M.; Yan, H. Challenges and Opportunities for Structural DNA Nanotechnology. *Nat. Nanotechnol.* **2011**, *6*, 763−772.

(8) Torring, T.; Voigt, N. V.; Nangreave, J.; Yan, H.; Gothelf, K. V. DNA Origami: A Quantum Leap for Self-Assembly of Complex Structures. *Chem. Soc. Rev.* **2011**, *40*, 5636−5646.

(9) Simmel, F. C. DNA-based Assembly Lines and Nanofactories. *Curr. Opin. Biotechnol.* **2012**, *23*, 516−521.

(10) Zhang, F.; Nangreave, J.; Liu, Y.; Yan, H. Structural DNA Nanotechnology: State of The Art and Future Perspective. *J. Am. Chem. Soc.* **2014**, *136*, 11198−211.

(11) He, Y.; Chen, Y.; Liu, H.; Ribbe, A. E.; Mao, C. Self-assembly of Hexagonal DNA Two-dimensional (2D) Arrays. *J. Am. Chem. Soc.* **2005**, *127*, 12202−3.

(12) Yurke, B.; Turberfield, A. J.; Mills, A. P.; Simmel, F. C.; Neumann, J. L. A DNA-fuelled Molecular Machine Made of DNA. *Nature* **2000**, *406*, 605−608.

(13) Chao, J.; Liu, H.; Su, S.; Wang, L.; Huang, W.; Fan, C. Structural DNA Nanotechnology for Intelligent Drug Delivery. *Small* **2014**, *10*, 4626.

(14) Tintore, M.; Eritja, R.; Fabrega, C. DNA Nanoarchitectures: Steps Towards Biological Applications. *ChemBioChem* **2014**, *15*, 1374−90.

(15) Khodakov, D.; Wang, C.; Zhang, D. Y. Diagnostics Based on Nucleic Acid Sequence Variant Profiling: PCR, Hybridization, and NGS Approaches. *Adv. Drug Delivery Rev.* **2016**, *105*, 3−19.

(16) Keum, J. W.; Bermudez, H. Enhanced Resistance of DNA Nanostructures to Enzymatic Digestion. *Chem. Commun. (Cambridge, U. K.)* **2009**, 7036−8.

(17) Mei, Q.; Wei, X.; Su, F.; Liu, Y.; Youngbull, C.; Johnson, R.; Lindsay, S.; Yan, H.; Meldrum, D. Stability of DNA Origami Nanoarrays in Cell Lysate. *Nano Lett.* **2011**, *11*, 1477−82.

(18) Conway, J. W.; McLaughlin, C. K.; Castor, K. J.; Sleiman, H. DNA Nanostructure Serum Stability: Greater Than The Sum of Its Parts. *Chem. Commun. (Cambridge, U. K.)* **2013**, *49*, 1172−4.

(19) Lee, H.; Lytton-Jean, A. K. R.; Chen, Y.; Love, K. T.; Park, A. I.; Karagiannis, E. D.; Sehgal, A.; Querbes, W.; Zurenko, C. S.; Jayaraman, M.; Peng, C. G.; Charisse, K.; Borodovsky, A.; Manoharan, M.; Donahoe, J. S.; Truelove, J.; Nahrendorf, M.; Langer, R.; Anderson, D. G. Molecularly Self-assembled Nucleic Acid Nanoparticles for Targeted In Vivo Sirna Delivery. *Nat. Nanotechnol.* **2012**, *7*, 389−393.

(20) Charoenphol, P.; Bermudez, H. Aptamer-Targeted DNA Nanostructures for Therapeutic Delivery. *Mol. Pharmaceutics* **2014**, *11*, 1721−1725.

(21) Liu, X. W.; Xu, Y.; Yu, T.; Clifford, C.; Liu, Y.; Yan, H.; Chang, Y. A DNA Nanostructure Platform for Directed Assembly of Synthetic Vaccines. *Nano Lett.* **2012**, *12*, 4254−4259.

(22) Jiang, Q.; Song, C.; Nangreave, J.; Liu, X. W.; Lin, L.; Qiu, D. L.; Wang, Z. G.; Zou, G. Z.; Liang, X. J.; Yan, H.; Ding, B. Q. DNA Origami as a Carrier for Circumvention of Drug Resistance. *J. Am. Chem. Soc.* **2012**, *134*, 13396−13403.

(23) Rudchenko, M.; Taylor, S.; Pallavi, P.; Dechkovskaia, A.; Khan, S.; Butler, V. P., Jr; Rudchenko, S.; Stojanovic, M. N. Autonomous Molecular Cascades for Evaluation of Cell Surfaces. *Nat. Nanotechnol.* **2013**, *8*, 580−586.

(24) Rothemund, P. W. K. Folding DNA to Create Nanoscale Shapes and Patterns. *Nature* **2006**, *440*, 297−302.

(25) Teichmann, M.; Kopperger, E.; Simmel, F. C. Robustness of Localized DNA Strand Displacement Cascades. *ACS Nano* **2014**, *8*, 8487−96.

(26) Kopperger, E.; Pirzer, T.; Simmel, F. C. Diffusive Transport of Molecular Cargo Tethered to a DNA Origami Platform. *Nano Lett.* **2015**, *15*, 2693−9.

(27) Ruiz, I. M.; Arbona, J. M.; Lad, A.; Mendoza, O.; Aime, J. P.; Elezgaray, J. Connecting Localized DNA Strand Displacement Reactions. *Nanoscale* **2015**, *7*, 12970−12978.

(28) Chandran, H.; Gopalkrishnan, N.; Phillips, A.; Reif, J. Localized Hybridization Circuits. In *DNA Computing and Molecular Programming*; Cardelli, L., Shih, W., Eds.; Springer: Berlin, Germany, 2011; Vol. *6937*, pp 64−83.

(29) Muscat, R. A.; Strauss, K.; Ceze, L.; Seelig, G. DNA-Based Molecular Architecture With Spatially Localized Components. In *ISCA '13: Proceedings of the 40th Annual International Symposium on Computer Architecture*; Mendelson, A., Ed.; ACM: Tel-Aviv, Israel, 2013; Vol. *41*, pp 177−188.

(30) Dalchau, N.; Chandran, H.; Gopalkrishnan, N.; Phillips, A.; Reif, J. Probabilistic Analysis of Localized DNA Hybridization Circuits. *ACS Synth. Biol.* **2015**, *4*, 898−913.

(31) Chatterjee, G.; Dalchau, N.; Muscat, R. A.; Phillips, A.; Seelig, G. A Spatially Localized Architecture for Fast and Modular DNA Computing. *Nat. Nanotechnol.* **2017**, *12*, 920−927.
(32) Bui, H.; Miao, V.; Garg, S.; Mokhtar, R.; Song, T.; Reif, J. Design and Analysis of Localized DNA Hybridization Chain Reactions. *Small* **2017**, *13*, 1602983.
(33) Zhang, D. Y.; Seelig, G. Dynamic DNA Nanotechnology Using Strand-Displacement Reactions. *Nat. Chem.* **2011**, *3*, 103−113.
(34) Dirks, R. M.; Pierce, N. A. Triggered Amplification by Hybridization Chain Reaction. *Proc. Natl. Acad. Sci. U. S. A.* **2004**, *101*, 15275−15278.
(35) Garg, S. Programming Molecular Devices Using Nucleic Acid Hairpins. Ph.D. Thesis, Duke University, 2016.
(36) Bui, H.; Garg, S.; Miao, V.; Song, T.; Mokhtar, R.; Reif, J. Design and Analysis of Linear Cascade DNA Hybridization Chain Reactions Using DNA Hairpins. *New J. Phys.* **2017**, *19*, 015006.
(37) Qian, L.; Winfree, E. Scaling Up Digital Circuit Computation with DNA Strand Displacement Cascades. *Science* **2011**, *332*, 1196−1201.
(38) Song, X.; Eshra, A.; Dwyer, C.; Reif, J. Renewable DNA Seesaw Logic Circuits Enabled by Photoregulation of Toehold-Mediated Strand Displacement. *RSC Adv.* **2017**, *7*, 28130−28144.
(39) Jungmann, R.; Steinhauer, C.; Scheible, M.; Kuzyk, A.; Tinnefeld, P.; Simmel, F. C. Single-Molecule Kinetics and Super-Resolution Microscopy by Fluorescence Imaging of Transient Binding on DNA Origami. *Nano Lett.* **2010**, *10*, 4756−4761.
(40) Vietz, C.; Lalkens, B.; Acuna, G. P.; Tinnefeld, P. Synergistic Combination of Unquenching and Plasmonic Fluorescence Enhancement in Fluorogenic Nucleic Acid Hybridization Probes. *Nano Lett.* **2017**, *17*, 6496−6500.
(41) Jungmann, R.; Avendaño, M. S.; Woehrstein, J. B.; Dai, M.; Shih, W. M.; Yin, P. Multiplexed 3D Cellular Super-Resolution Imaging with DNA-PAINT and Exchange-PAINT. *Nat. Methods* **2014**, *11*, 313−318.
(42) Zhang, D. Y.; Winfree, E. Control of DNA Strand Displacement Kinetics Using Toehold Exchange. *J. Am. Chem. Soc.* **2009**, *131*, 17303−17314.
(43) Hua, B.; Han, K. Y.; Zhou, R.; Kim, H.; Shi, X.; Abeysirigunawardena, S. C.; Jain, A.; Singh, D.; Aggarwal, V.; Woodson, S. A. An Improved Surface Passivation Method for Single-Molecule Studies. *Nat. Methods* **2014**, *11*, 1233−1236.
(44) Pan, H.; Xia, Y.; Qin, M.; Cao, Y.; Wang, W. A Simple Procedure to Improve the Surface Passivation for Single Molecule Fluorescence Studies. *Phys. Biol.* **2015**, *12*, 045006.
(45) Ovesný, M.; Křížek, P.; Borkovec, J.; Švindrych, Z.; Hagen, G. M. ThunderSTORM: A Comprehensive ImageJ Plug-in for PALM and STORM Data Analysis and Super-Resolution Imaging. *Bioinformatics* **2014**, *30*, 2389−2390.

DOI: 10.1021/acsnano.7b06699
ACS Nano 2018, 12, 1146−1155